# Liquid crystal phase formation for the linear tangent hard sphere model from Monte Carlo simulations

Carlos Vega, Carl McBride, and Luis G. MacDowell[a)]
*Departamento de Química Física, Facultad de Ciencias Químicas, Universidad Complutense de Madrid, Ciudad Universitaria 28040 Madrid, Spain*

(Received 30 April 2001; accepted 8 June 2001)

Monte Carlo simulations have been performed for the linear tangent hard sphere model. The models considered in this work consisted of $m=3$, 4, 5, 6, and 7 monomer units. For the models $m=3$ and $m=4$ we find an isotropic fluid and an ordered solid. For the $m=5$ model we find the sequence of phases isotropic–nematic–smectic A on compression, and the sequence solid–smectic A–isotropic on expansion. We suggest that the nematic phase for this model is meta stable. For the model $m=6$ we observe the phase sequence isotropic–nematic–smectic A on compression, and the sequence ordered solid–smectic A–nematic–isotropic on expansion. We observe a similar sequence on expansion of the $m=7$ model. The results for the $m=7$ model are in good agreement with those of Williamson and Jackson [J. Chem. Phys. **108**, 10294 (1998)]. It was suggested by Flory [Proc. R. Soc. London, Ser. A **234**, 73 (1956)] that liquid crystal phases could exist for length to breadth ratios $\geqslant 5.437$, i.e., $m\geqslant 6$. In this work we place the lower bound at $m\geqslant 5$. © *2001 American Institute of Physics.* [DOI: 10.1063/1.1389095]

## I. INTRODUCTION

Onsager-type theories[1] of liquid crystal phase formation often examine the competition between positional and orientational entropy. A molecule that has nonspherical symmetry has an excluded volume that also displays nonspherical symmetry. For gases and low density liquids molecules are free to adopt almost any position and orientation. As the density increases and molecules enter in close proximity to one another it is found that a loss of orientational freedom is more than offset by the positional freedom that alignment affords. The density, or packing fraction, at which it becomes more profitable for the system to become aligned very much depends on the degree of anisotropy of the constituent particles. For infinitely long rods this transition to an orientationally ordered phase (i.e., a *nematic* phase) occurs at a vanishingly small density. However, for particles whose anisotropy is very small the fluid–solid transition occurs before any orientational transition. It should be mentioned that Onsager-type theories are at their best for dilute solutions. This is due to the neglect of higher order terms in the virial expansion used to calculate the free energy.

Another class of theories designed to explain the isotropic–nematic transition are lattice theories. One of the major proponents of lattice theories was Flory.[2] In lattice theories one may derive the partition function of a system by examining the number of configurations that are available to a model consisting of a number of lattice points. The advantage of lattice theories over Onsager-type expansions of the free energy is the fact that the lattice models are applicable over the whole range of concentrations. Flory used a number of arguments in order to derive a lower limit for the formation of an orientationally ordered phase. When the bond length is equal to the hard sphere diameter then the model is known as the linear tangent hard sphere model (LTHS). One of the lowest estimates arrived at was for a molecular length to breadth ratio of $2e$ (i.e., 5.437), thus suggesting that the first LTHS model to demonstrate liquid crystal behavior would be the case $m=6$ where $m$ is the number of monomers in the model. More recently Chamoux and Perera[3] have extrapolated integral equation results for the hypernetted chain equation and have arrived at the conclusion that an isotropic–nematic transition should occur for $m>7$.

In recent years computer simulation of liquid crystal phases at the molecular or atomistic level has proved increasingly useful as an aid to understanding this interesting state of matter. One of the fundamental requirements of a mesogenic molecule is a strong shape anisotropy. To this end there exist numerous examples of simulations whose main feature is shape anisotropy. Popular models for such simulations have been spherocylinders,[4–7] and spheroids of revolution.[8,9] As well as simulations where the molecules are geometric bodies, one has models that are built up of a number of geometric units. One such unit is the hard sphere. A series of $m$ hard spheres can be used to construct a linear configuration thus representing a molecule. Another interesting model is the fused hard sphere model as used by Whittle and Masters.[10] In the fused hard sphere model the configuration is again linear, however, the bond length is now less than the hard sphere diameter. Recently Jaffer *et al.*[11] have developed Flory dimer theory to study the nematic–isotropic transition of this model.

The authors Yethiraj and Fynewever have studied the isotropic–nematic transition for the LTHS models with $m=8$ and $m=20$.[12,13] Williamson and Jackson[14] have undertaken extensive simulations of the $m=7$ case and found

[a)]Present address: Johannes Gutenberg–Universitat Mainz, Institut fur Physik, WA31, D-55099, Mainz, Germany.

 

nematic and smectic phases as well as the isotropic and solid phases. The appearance of the smectic phase is particularly interesting since it indicates that LTHS model has more in common with spherocylinders than with ellipsoids (smectic phases are not observed in the hard ellipsoid model). Wilson,[15] considered the case of a model with $m=5$ spheres. Using a rattling sphere molecular dynamics method[16,17] for the hard monomer components a degree of flexibility was introduced into the LTHS model. For the least flexible models a meta stable smectic phase was found.

In this paper we shall study the LTHS model for $m=3$, 4, 5, 6, and 7. Using the first order thermodynamic perturbation theory of Wertheim[18,19] (TPT1) to provide an isotropic equation of state (EOS) a comparison will be made to the simulation results. In 1994 Vega and Lago[20] developed a theory to describe the isotropic–nematic transition. With the aid of a reliable equation of state for the isotropic phase a rescaling approximation for the virial coefficients in the nematic phase is made. A suitable EOS for the LTHS model in the isotropic phase was proposed by Vega *et al.*[21] This EOS, in conjunction with the analytical expression for the excluded volume of the LTHS model (Williamson and Jackson[22]) will be used to provide theoretical estimates of the location of the isotropic–nematic transition for each of the models examined.

The scheme of the paper is as follows. In Sec. II the simulation methodology and models will be presented. In Sec. III the simulations results will be presented. Finally, our conclusions are presented in Sec. IV.

## II. MODEL AND COMPUTATIONAL TECHNIQUE

The molecular model used in this work consists of $m$ rigid tangent hard spheres (or monomers) in a linear configuration. Each of the monomers are of diameter $\sigma$. The bond length between monomers is set at $L=\sigma$. Monomers in different molecules interact via a hard sphere potential.[23] Intramolecular interactions between monomers of the same molecule were also considered, thus preventing the overlap of one molecule with its periodic image when simulating a small number of molecules. Since all the interactions in the model are hard interactions the temperature becomes a redundant variable and the properties of the system depend only on density.

In this work we have considered the LTHS models consisting of $m=3$, 4, 5, 6, and 7 hard spheres. The simulations were performed using the Monte Carlo method in the $NpT$ ensemble. Two sets of simulation runs were performed; one set was of $N=144$ molecules with approximately $3\times10^5$ cycles for equilibration followed by $3\times10^5$ cycles for production averages. The other set consisted of a larger system, with $N=320$ for compression runs and $N=324$ for expansion runs. Simulations of the larger systems consisted of $1.5\times10^5$ cycles for equilibration followed by $8.5\times10^5$ cycles for production averages. A MC cycle includes a trial move per particle (translation 50%, rotation 50%) plus a trial volume change.

The compression runs were started from a very low density state. The initial configuration was that of the $\alpha N_2$-face centered cubic structure[23] which has four molecules in the unit cell. The $N=320$ system consisted of $4\times4\times5$ of these unit cells. Thus the initial nematic order parameter was zero and no preferential direction to the molecules was artificially introduced. Within a few steps the solid melted and transformed into a low density isotropic fluid. The fluid is then compressed by increasing the pressure. The last configuration from a certain pressure was used as initial configuration for the next, higher, pressure. States for which the nematic order parameter was greater than 0.4 were classified as being nematic. Throughout the compression runs isotropic scaling was applied to the simulation box.

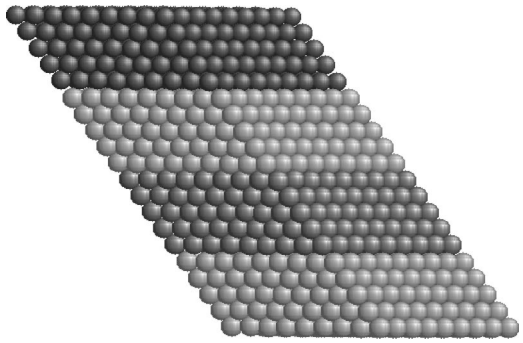

FIG. 1. An example of an initial solid phase starting configuration. Shading is applied to individual layers as a visual aid.

The expansion runs were started from a high density solid. The high density solid is obtained starting from a close packed fcc structure of hard spheres with stacking sequence ABCABC (see Fig. 1). The molecules are constructed by linking $m$ monomers in a linear configuration. The same orientation is assigned to all of the molecules in each of the layers. The final solid structure corresponds to the CP1 structure in the paper by Vega *et al.*[24] on the solid phases of hard dumbbells. Notice that the molecular axis is tilted with respect to the layer normal (i.e., the $A$ plane of the fcc hard sphere solid). The $N=324$ system consisted of 4 layers of $9\times9$ molecules. The expansion runs were started from a high density closed packed solid and therefore our simulation box is not cubic. Nonisotropic $NpT$ Monte Carlo[25,26] was used. The simulation box was free to change shape (i.e., box side lengths and angles). This is important when simulating solid phases and it is likely to also be true for smectic phases. Expansion runs were performed starting from a high density solid at very high pressure and then gradually decreasing the pressure.

During the simulations the nematic order parameter (which is zero for an isotropic fluid and one for a perfectly aligned system) was continuously monitored. This was done by first calculating a director vector[27]

$$Q_{\alpha\beta}=\frac{1}{N}\sum_{j=1}^{N}\left(\frac{3}{2}\hat{\mathbf{e}}_{j\alpha}\hat{\mathbf{e}}_{j\beta}-\frac{1}{2}\delta_{\alpha\beta}\right),\quad \alpha,\beta=x,y,z, \tag{1}$$

where $Q$ is a second rank tensor, $\hat{\mathbf{e}}_j$ is a unit vector along the molecular long axis, and $\delta_{\alpha\beta}$ is the Kronecker delta. Diagonalization of this tensor gives three eigenvalues $\lambda_+$, $\lambda_0$, and $\lambda_-$, and $\mathbf{n}$ is the eigenvector associated with the largest eigenvalue ($\lambda_+$). From this director vector the nematic order parameter is calculated from[28]

TABLE I. Equation of state for the 3 LTHS model from $NpT$ MC simulations (expansion route). The reduced pressure $p^*$ is defined as $p^* = p\sigma^3/(kT)$, $Z$ stands for the compressibility factor, $y$ for the volume fraction. The different phases have been labeled as $I$ (isotropic) and $K$ (crystalline solid).

| $p^*$ | $y$ | $Z$ | No. molecules | Phase |
|---|---|---|---|---|
| 130 | 0.727 | 280.78 | 144 | $K$ |
| 110 | 0.725 | 238.46 | 144 | $K$ |
| 90 | 0.722 | 195.91 | 144 | $K$ |
| 70 | 0.717 | 153.44 | 144 | $K$ |
| 50 | 0.707 | 111.01 | 144 | $K$ |
| 40 | 0.699 | 89.87 | 144 | $K$ |
| 30 | 0.685 | 68.74 | 144 | $K$ |
| 20 | 0.664 | 47.34 | 144 | $K$ |
| 15 | 0.640 | 36.83 | 144 | $K$ |
| 10 | 0.599 | 26.23 | 144 | $K$ |
| 9 | 0.588 | 24.03 | 144 | $K$ |
| 8 | 0.569 | 22.07 | 144 | $K$ |
| 7 | 0.554 | 19.85 | 144 | $K$ |
| 6 | 0.529 | 17.83 | 144 | $K$ |
| 5 | 0.430 | 18.28 | 144 | $I$ |

$$S_2 = \lambda_+ = \langle P_2(\mathbf{n}\cdot\mathbf{e})\rangle = \langle P_2(\cos\theta)\rangle = \langle \tfrac{3}{2}\cos^2\theta - \tfrac{1}{2}\rangle, \quad (2)$$

where $S_2$ is known as the uniaxial order parameter. Here $P_2$ is the second order Legendre polynomial, $\theta$ is the angle between a molecular axes and the director $\mathbf{n}$, and the angle brackets indicate an ensemble average. As well as the nematic order parameter snapshots of simulation configurations were also taken for use as an aid to phase identification.

The simulation results in the isotropic branch are compared with the theoretical EOS, known as first order thermodynamic perturbation theory[18,19] (TPT1) which is given by

$$Z = \frac{p}{\rho kT} = m\frac{1+y+y^2-y^3}{(1-y)^3} - (m-1)\frac{1+y-(y^2/2)}{(1-y)[1-(y/2)]}, \quad (3)$$

where $m$ is the number of tangent hard spheres forming the chain and $y$ is the volume fraction defined as

$$y = \rho V_m = \rho\frac{\pi\sigma^3 m}{6}, \quad (4)$$

where $\rho = N/V$ is the number density of molecules and $V_m$ is the molecular volume.

The theoretical results for the location of the isotropic–nematic transition are obtained from the Vega–Lago theory[20] using the EOS:[21]

$$Z = \frac{1+k_1 y+k_2 y^2+k_3 y^3}{(1-y^3)} + (B_4^{*,\mathrm{exact}} - B_4^{*,\mathrm{theor}})y^3, \quad (5)$$

where

$$k_1 = B_2^* - 3, \quad (6)$$

$$k_2 = B_3^* - 3B_2^* + 3, \quad (7)$$

$$k_3 = (B_5^* - 6B_3^* + 8B_2^* - 3)/3, \quad (8)$$

TABLE II. Equation of state for the 4 LTHS model from $NpT$ MC simulations (compression route). The reduced pressure $p^*$ is defined as $p^* = p\sigma^3/(kT)$, $Z$ stands for the compressibility factor, $y$ for the volume fraction, $S_2$ for the order parameter. The phases have been labeled as $I$ (isotropic). The horizontal line divides the results for the $N=144$ results from the $N=320$ results.

| $p^*$ | $y$ | $Z$ | $S_2$ | No. molecules | Phase |
|---|---|---|---|---|---|
| 0.1 | 0.097 | 2.16 | 0.06 | 144 | $I$ |
| 0.2 | 0.140 | 2.99 | 0.09 | 144 | $I$ |
| 0.4 | 0.192 | 4.36 | 0.06 | 144 | $I$ |
| 0.6 | 0.226 | 5.56 | 0.10 | 144 | $I$ |
| 0.8 | 0.251 | 6.67 | 0.09 | 144 | $I$ |
| 1.0 | 0.271 | 7.72 | 0.04 | 144 | $I$ |
| 1.2 | 0.290 | 8.66 | 0.12 | 144 | $I$ |
| 1.4 | 0.305 | 9.61 | 0.10 | 144 | $I$ |
| 1.6 | 0.316 | 10.60 | 0.10 | 144 | $I$ |
| 1.8 | 0.329 | 11.44 | 0.07 | 144 | $I$ |
| 2.0 | 0.341 | 12.30 | 0.06 | 144 | $I$ |
| 2.2 | 0.350 | 13.16 | 0.09 | 144 | $I$ |
| 2.4 | 0.359 | 13.99 | 0.09 | 144 | $I$ |
| 2.6 | 0.369 | 14.75 | 0.13 | 144 | $I$ |
| 2.8 | 0.376 | 15.62 | 0.10 | 144 | $I$ |
| 3.0 | 0.383 | 16.41 | 0.14 | 144 | $I$ |
| 3.2 | 0.392 | 17.09 | 0.09 | 144 | $I$ |
| 0.3 | 0.169 | 3.71 | 0.09 | 320 | $I$ |
| 0.8 | 0.252 | 6.66 | 0.09 | 320 | $I$ |
| 1.8 | 0.329 | 11.44 | 0.08 | 320 | $I$ |
| 2.9 | 0.380 | 15.98 | 0.06 | 320 | $I$ |
| 3.2 | 0.392 | 17.08 | 0.14 | 320 | $I$ |
| 3.5 | 0.401 | 18.27 | 0.09 | 320 | $I$ |
| 3.6 | 0.406 | 18.55 | 0.14 | 320 | $I$ |
| 3.7 | 0.410 | 18.92 | 0.09 | 320 | $I$ |
| 3.8 | 0.411 | 19.36 | 0.11 | 320 | $I$ |
| 3.9 | 0.416 | 19.65 | 0.12 | 320 | $I$ |
| 4.0 | 0.417 | 20.09 | 0.05 | 320 | $I$ |
| 4.1 | 0.422 | 20.35 | 0.15 | 320 | $I$ |
| 4.2 | 0.426 | 20.66 | 0.08 | 320 | $I$ |
| 4.3 | 0.426 | 21.15 | 0.14 | 320 | $I$ |
| 4.4 | 0.429 | 21.46 | 0.05 | 320 | $I$ |
| 4.6 | 0.437 | 22.03 | 0.13 | 320 | $I$ |
| 4.8 | 0.444 | 22.66 | 0.16 | 320 | $I$ |
| 4.9 | 0.449 | 22.88 | 0.15 | 320 | $I$ |
| 5.0 | 0.451 | 23.23 | 0.12 | 320 | $I$ |
| 5.1 | 0.457 | 23.35 | 0.11 | 320 | $I$ |
| 5.2 | 0.461 | 23.60 | 0.12 | 320 | $I$ |
| 5.3 | 0.468 | 23.71 | 0.12 | 320 | $I$ |
| 5.5 | 0.473 | 24.36 | 0.15 | 320 | $I$ |
| 5.7 | 0.481 | 24.83 | 0.15 | 320 | $I$ |
| 5.9 | 0.493 | 25.08 | 0.12 | 320 | $I$ |
| 6.0 | 0.495 | 25.39 | 0.13 | 320 | $I$ |

$$B_4^{*,\mathrm{theor}} = k_3 + 3k_2 + 6k_1 + 10, \quad (9)$$

and

$$B_i^* = \frac{B_i}{V_m^{i-1}}, \quad (10)$$

where $B_i$ is the $i$th virial coefficient. The EOS described by Eq. (5) is used in preference to the TPT1 EOS due to its improved prediction of the compressibility at high packing fractions, i.e., close to the isotropic–nematic transition. This EOS is used in conjunction with the exact expression for the excluded volume of the LTHS model provided by Williamson and Jackson.[22]

TABLE III. Equation of state for the 4 LTHS model from $NpT$ MC simulations (expansion route). The reduced pressure $p^*$ is defined as $p^*=p\sigma^3/(kT)$, $Z$ stands for the compressibility factor, $y$ for the volume fraction, $S_2$ for the order parameter. The different phases have been labeled as $I$ (isotropic) and $K$ (crystalline solid).

| $p^*$ | $y$ | $Z$ | $S_2$ | No. molecules | Phase |
|---|---|---|---|---|---|
| 130.0 | 0.731 | 372.71 | 0.99 | 144 | $K$ |
| 110.0 | 0.729 | 316.09 | 0.99 | 144 | $K$ |
| 90.0 | 0.726 | 259.59 | 0.99 | 144 | $K$ |
| 70.0 | 0.722 | 202.96 | 0.99 | 144 | $K$ |
| 50.0 | 0.716 | 146.33 | 0.99 | 144 | $K$ |
| 40.0 | 0.708 | 118.27 | 0.99 | 144 | $K$ |
| 30.0 | 0.699 | 89.87 | 0.99 | 144 | $K$ |
| 20.0 | 0.680 | 61.60 | 0.99 | 144 | $K$ |
| 15.0 | 0.663 | 47.41 | 0.99 | 144 | $K$ |
| 10.0 | 0.631 | 33.19 | 0.99 | 144 | $K$ |
| 9.0 | 0.619 | 30.46 | 0.99 | 144 | $K$ |
| 8.0 | 0.606 | 27.63 | 0.99 | 144 | $K$ |
| 7.0 | 0.590 | 24.86 | 0.99 | 144 | $K$ |
| 6.0 | 0.572 | 21.96 | 0.99 | 144 | $K$ |
| 5.0 | 0.543 | 19.30 | 0.98 | 144 | $K$ |
| 4.8 | 0.540 | 18.63 | 0.98 | 144 | $K$ |
| 4.6 | 0.534 | 18.05 | 0.98 | 144 | $K$ |
| 4.4 | 0.523 | 17.64 | 0.98 | 144 | $K$ |
| 4.2 | 0.512 | 17.17 | 0.97 | 144 | $K$ |
| 4.0 | 0.505 | 16.58 | 0.97 | 144 | $K$ |
| 3.8 | 0.484 | 16.45 | 0.94 | 144 | $K$ |
| 3.6 | 0.412 | 18.30 | 0.04 | 144 | $I$ |
| 3.4 | 0.399 | 17.83 | 0.06 | 144 | $I$ |
| 3.2 | 0.390 | 17.18 | 0.11 | 144 | $I$ |
| 3.0 | 0.381 | 16.49 | 0.04 | 144 | $I$ |
| 2.8 | 0.378 | 15.50 | 0.05 | 144 | $I$ |
| 2.6 | 0.370 | 14.72 | 0.09 | 144 | $I$ |
| 2.4 | 0.358 | 14.03 | 0.10 | 144 | $I$ |
| 2.2 | 0.347 | 13.27 | 0.05 | 144 | $I$ |
| 2.0 | 0.343 | 12.20 | 0.08 | 144 | $I$ |
| 1.8 | 0.331 | 11.39 | 0.06 | 144 | $I$ |
| 1.6 | 0.318 | 10.55 | 0.09 | 144 | $I$ |
| 1.4 | 0.305 | 9.60 | 0.13 | 144 | $I$ |
| 1.2 | 0.289 | 8.69 | 0.11 | 144 | $I$ |
| 1.0 | 0.271 | 7.72 | 0.08 | 144 | $I$ |
| 0.8 | 0.252 | 6.64 | 0.08 | 144 | $I$ |
| 0.6 | 0.228 | 5.52 | 0.07 | 144 | $I$ |

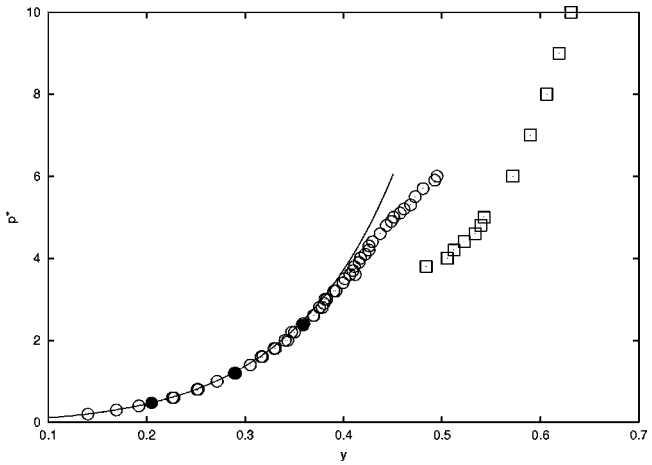


FIG. 2. Plot of the EOS for the 4 LTHS model. ⊙ represents isotropic state points, ⊡ represents solid state points. The solid curve is the TPT1 EOS. The ● points represent the results of Boublik *et al.* (Ref. 31).

## III. SIMULATION RESULTS

### A. The $m=3$ model

The results for the expansion branch of the trimer model are given in Table I. The trimer results locate the solid–isotropic transition at a packing fraction of between ($0.430 \leqslant y \leqslant 0.529$). Results for the trimer model in the liquid phase have been published previously (see Amos and Jackson[29] and also Müller and Gubbins[30]). No mesophases are observed for the trimer model.

### B. The $m=4$ model

In Tables II and III the simulation results for the compression and expansion runs of the tetramer model are reported. In Fig. 2 the EOS as obtained from simulation is presented along with the results of Boublik *et al.*[31] The prediction for the location of the isotropic–nematic transition from the Vega–Lago theory is given in Table IV.

From Fig. 2 it can be seen that TPT1 describes the simulation results of the isotropic phase up to $y=0.3$ rather well but overestimates the simulation results at higher packing fractions. A kink is observed in the isotropic branch at $y=0.45$. The states obtained for higher densities are isotropic but of glassy nature indicating the tendency of the system to freeze. This is further confirmed by expansion of the highest state obtained in the compression run. The system forms a hysteresis loop returning to the isotropic branch only at $p^*=p/(kT/\sigma^3)=4.4$, $y=0.43$.

In the solid phase the molecules are tilted with respect to the direction perpendicular to the layer (Fig. 1). This angle changes from 35 degrees at very high densities to 30 degrees for the densities close to melting. Similar behavior has been observed for hard dumbbells ($m=2$).[24] At a reduced pressure of $p^*=3.6$ the solid becomes mechanically unstable and transforms spontaneously into an isotropic fluid. Further expansion of this isotropic fluid gives an EOS indistinguishable of that obtained in the compression runs.

Therefore, for the tetramer, we only observe an isotropic fluid and an ordered solid. The fluid–solid transition must occur at a reduced pressure between 3.6 and 5.4. As a first approximation one may say the the fluid–solid transition occurs at $p^*=4.2$ for the tetramer. A more precise location would require free energy calculations for the solid phase.

It is interesting to note that for the tetramer the Vega–Lago theory predicts an isotropic–nematic transition at a pressure of 4.35.

### C. The $m=5$ case

In Fig. 3 we plot the EOS for the pentamer model ($m=5$). Once again it is seen that TPT1 provides a good description of the isotropic EOS up to a packing fraction of $y=0.30$. For packing fractions greater than this value TPT1 starts to overestimate the pressure.

Expansion of the solid configuration gives the following phase behavior; we find that the initial solid phase stable down to $y=0.478$, which melted into the liquid crystal smectic A phase ($0.415 \leqslant y \leqslant 0.474$). Below $y=0.396$ we find the isotropic fluid. A snapshot of the smectic A configu-

TABLE IV. Results from the Vega–Lago theory for the prediction of the isotropic nematic transition.

| | $p^*$ | $y_{\text{isotropic}}$ | $y_{\text{nematic}}$ |
|---|---|---|---|
| $m=4$ | 4.350 | 0.429 | 0.440 |
| $m=5$ | 2.095 | 0.357 | 0.370 |
| $m=6$ | 1.235 | 0.304 | 0.318 |
| $m=7$ | 0.820 | 0.262 | 0.277 |

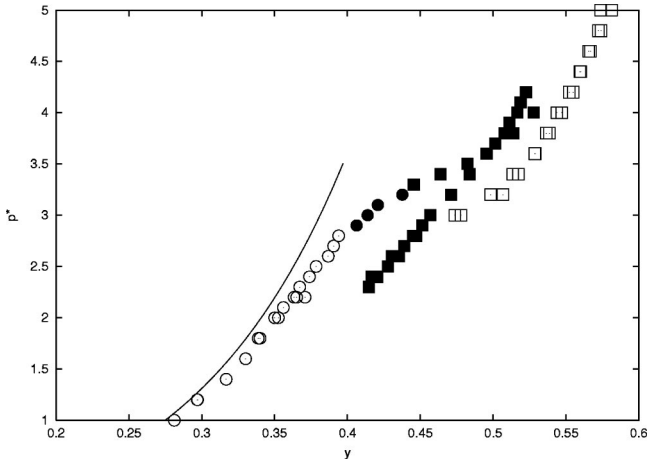


FIG. 3. Plot of the EOS for the 5 LTHS model. ⊙ represents isotropic state points, ● represents nematic state points, ■ represents smectic state points, and ⊡ represents solid state points. The solid curve is the TPT1 EOS.

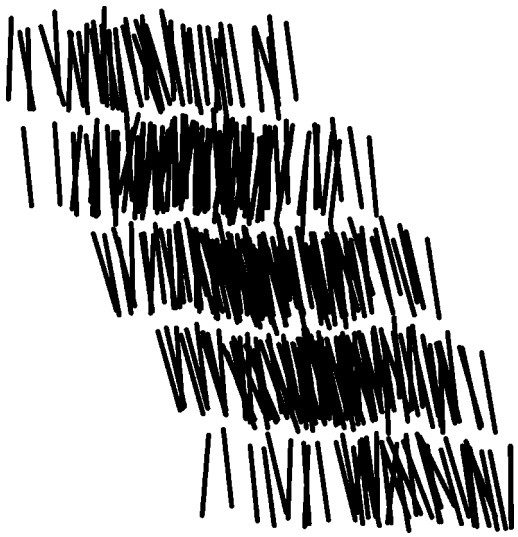

FIG. 4. Snapshot of the 5 LTHS system in the smectic A phase at a packing fraction 0.451, $p^*=2.9$. In this figure the molecules are represented by rods as a visual aid.

TABLE V. Equation of state for the 5 LTHS model from $NpT$ MC simulations (compression route). The reduced pressure $p^*$ is defined as $p^*=p\sigma^3/(kT)$, $Z$ stands for the compressibility factor, $y$ for the volume fraction, $S_2$ for the order parameter. The different phases have been labeled as $I$ (isotropic), $N$ (nematic), and Sm A (smectic A). The horizontal line divides the results for the $N=144$ results from the $N=320$ results.

| $p^*$ | $y$ | $Z$ | $S_2$ | No. molecules | Phase |
|---|---|---|---|---|---|
| 0.1 | 0.104 | 2.53 | 0.06 | 144 | $I$ |
| 0.2 | 0.148 | 3.54 | 0.09 | 144 | $I$ |
| 0.4 | 0.199 | 5.26 | 0.10 | 144 | $I$ |
| 0.6 | 0.232 | 6.76 | 0.07 | 144 | $I$ |
| 0.8 | 0.257 | 8.16 | 0.09 | 144 | $I$ |
| 1.0 | 0.279 | 9.40 | 0.07 | 144 | $I$ |
| 1.2 | 0.298 | 10.53 | 0.11 | 144 | $I$ |
| 1.4 | 0.313 | 11.72 | 0.13 | 144 | $I$ |
| 1.6 | 0.327 | 12.81 | 0.10 | 144 | $I$ |
| 1.8 | 0.339 | 13.91 | 0.07 | 144 | $I$ |
| 2.0 | 0.353 | 14.83 | 0.06 | 144 | $I$ |
| 2.2 | 0.367 | 15.70 | 0.09 | 144 | $I$ |
| 0.3 | 0.176 | 4.47 | 0.07 | 320 | $I$ |
| 0.8 | 0.259 | 8.10 | 0.08 | 320 | $I$ |
| 1.2 | 0.297 | 10.57 | 0.13 | 320 | $I$ |
| 1.8 | 0.340 | 13.86 | 0.11 | 320 | $I$ |
| 2.0 | 0.350 | 14.96 | 0.14 | 320 | $I$ |
| 2.2 | 0.363 | 15.85 | 0.19 | 320 | $I$ |
| 2.3 | 0.367 | 16.39 | 0.13 | 320 | $I$ |
| 2.4 | 0.374 | 16.80 | 0.07 | 320 | $I$ |
| 2.5 | 0.379 | 17.29 | 0.14 | 320 | $I$ |
| 2.6 | 0.387 | 17.59 | 0.26 | 320 | $I$ |
| 2.7 | 0.391 | 18.10 | 0.26 | 320 | $I$ |
| 2.8 | 0.394 | 18.60 | 0.32 | 320 | $I$ |
| 2.9 | 0.406 | 18.69 | 0.45 | 320 | $N$ |
| 3.0 | 0.414 | 18.98 | 0.61 | 320 | $N$ |
| 3.1 | 0.421 | 19.28 | 0.63 | 320 | $N$ |
| 3.2 | 0.438 | 19.14 | 0.64 | 320 | $N$ |
| 3.3 | 0.446 | 19.39 | 0.67 | 320 | Sm A |
| 3.4 | 0.464 | 19.19 | 0.69 | 320 | Sm A |
| 3.5 | 0.482 | 19.00 | 0.69 | 320 | Sm A |
| 3.6 | 0.495 | 19.02 | 0.71 | 320 | Sm A |
| 3.7 | 0.502 | 19.31 | 0.69 | 320 | Sm A |
| 3.8 | 0.508 | 19.58 | 0.70 | 320 | Sm A |
| 3.9 | 0.511 | 19.98 | 0.69 | 320 | Sm A |
| 4.0 | 0.517 | 20.27 | 0.70 | 320 | Sm A |
| 4.1 | 0.519 | 20.68 | 0.70 | 320 | Sm A |
| 4.2 | 0.523 | 21.04 | 0.70 | 320 | Sm A |

ration for $y=0.451$ is given in Fig. 4. On compression we find the following phase behavior; we have an isotropic phase up to $y=0.394$, we obtain a nematic phase in the narrow range $(0.406 \leqslant y \leqslant 0.438)$, and above $y=0.446$ we have a smectic A phase. From the phase sequence on expansion, and the location and width of the nematic phase on compression, we suggest that the isotropic–nematic phase transition is meta stable with respect to the isotropic–smectic A phase transition. It is interesting to note that for a spherocylinder model of similar aspect ratio a direct isotropic–smectic A phase transition is also observed.[7] The compression run state points are given in Table V and the expansion run state points are given in Table VI. The Vega–Lago theory (see Table IV) provides us with an isotropic–nematic transition at a pressure $p^*=2.095$ which is below the $I$–$N$ transition seen on compression ($p^* \approx 2.8$).

In an attempt to clarify the order of the solid–smectic A

TABLE VI. Equation of state for the 5 LTHS model from $NpT$ MC simulations (expansion route). The reduced pressure $p^*$ is defined as $p^* = p\sigma^3/(kT)$, $Z$ stands for the compressibility factor, $y$ for the volume fraction, $S_2$ for the order parameter. The different phases have been labeled as $I$ (isotropic), Sm A (smectic A), and $K$ (crystalline solid). The horizontal line divides the results for the $N=144$ results from the $N=324$ results.

| $p^*$ | $y$ | $Z$ | $S_2$ | No. molecules | Phase |
|---|---|---|---|---|---|
| 130.0 | 0.731 | 465.45 | 0.99 | 144 | $K$ |
| 110.0 | 0.731 | 393.98 | 0.99 | 144 | $K$ |
| 90.0 | 0.729 | 323.16 | 0.99 | 144 | $K$ |
| 70.0 | 0.725 | 252.62 | 0.99 | 144 | $K$ |
| 50.0 | 0.720 | 181.82 | 0.99 | 144 | $K$ |
| 40.0 | 0.715 | 146.41 | 0.99 | 144 | $K$ |
| 30.0 | 0.707 | 111.03 | 0.99 | 144 | $K$ |
| 20.0 | 0.691 | 75.76 | 0.99 | 144 | $K$ |
| 15.0 | 0.677 | 57.98 | 0.99 | 144 | $K$ |
| 10.0 | 0.649 | 40.32 | 0.99 | 144 | $K$ |
| 6.0 | 0.600 | 26.17 | 0.99 | 144 | $K$ |
| 5.0 | 0.574 | 22.81 | 0.99 | 144 | $K$ |
| 4.8 | 0.572 | 21.96 | 0.99 | 144 | $K$ |
| 4.6 | 0.565 | 21.30 | 0.99 | 144 | $K$ |
| 4.4 | 0.559 | 20.59 | 0.99 | 144 | $K$ |
| 4.2 | 0.552 | 19.91 | 0.99 | 144 | $K$ |
| 4.0 | 0.544 | 19.26 | 0.99 | 144 | $K$ |
| 3.8 | 0.536 | 18.55 | 0.99 | 144 | $K$ |
| 3.6 | 0.529 | 17.82 | 0.99 | 144 | $K$ |
| 3.4 | 0.513 | 17.34 | 0.96 | 144 | $K$ |
| 3.2 | 0.498 | 16.82 | 0.97 | 144 | $K$ |
| 3.0 | 0.478 | 16.43 | 0.98 | 144 | $K$ |
| 2.8 | 0.446 | 16.43 | 0.93 | 144 | Sm A |
| 2.6 | 0.435 | 15.63 | 0.93 | 144 | Sm A |
| 2.4 | 0.420 | 14.94 | 0.90 | 144 | Sm A |
| 2.3 | 0.415 | 14.52 | 0.91 | 144 | Sm A |
| 2.2 | 0.371 | 15.53 | 0.26 | 144 | $I$ |
| 2.0 | 0.353 | 14.85 | 0.15 | 144 | $I$ |
| 1.8 | 0.339 | 13.91 | 0.13 | 144 | $I$ |
| 1.6 | 0.330 | 12.69 | 0.12 | 144 | $I$ |
| 1.4 | 0.317 | 11.57 | 0.11 | 144 | $I$ |
| 1.2 | 0.297 | 10.58 | 0.11 | 144 | $I$ |
| 1.0 | 0.281 | 9.31 | 0.11 | 144 | $I$ |
| 0.8 | 0.258 | 8.12 | 0.12 | 144 | $I$ |
| 0.6 | 0.232 | 6.78 | 0.11 | 144 | $I$ |
| 5.0 | 0.581 | 22.52 | 0.99 | 324 | $K$ |
| 4.8 | 0.574 | 21.89 | 0.98 | 324 | $K$ |
| 4.6 | 0.567 | 21.24 | 0.99 | 324 | $K$ |
| 4.4 | 0.560 | 20.56 | 0.98 | 324 | $K$ |
| 4.2 | 0.555 | 19.81 | 0.98 | 324 | $K$ |
| 4.0 | 0.547 | 19.14 | 0.98 | 324 | $K$ |
| 3.8 | 0.539 | 18.47 | 0.98 | 324 | $K$ |
| 3.6 | 0.529 | 17.83 | 0.98 | 324 | $K$ |
| 3.4 | 0.517 | 17.20 | 0.97 | 324 | $K$ |
| 3.2 | 0.507 | 16.53 | 0.96 | 324 | $K$ |
| 3.0 | 0.474 | 16.58 | 0.87 | 324 | $K$/Sm A |
| 2.9 | 0.451 | 16.82 | 0.89 | 324 | Sm A |
| 2.8 | 0.445 | 16.47 | 0.91 | 324 | Sm A |
| 2.7 | 0.439 | 16.10 | 0.74 | 324 | Sm A |
| 2.6 | 0.430 | 15.81 | 0.87 | 324 | Sm A |
| 2.5 | 0.428 | 15.30 | 0.87 | 324 | Sm A |
| 2.4 | 0.417 | 15.08 | 0.87 | 324 | Sm A |
| 2.3 | 0.396 | 15.20 | 0.34 | 324 | $I$ |
| 2.2 | 0.365 | 15.77 | 0.19 | 324 | $I$ |
| 2.1 | 0.356 | 15.44 | 0.14 | 324 | $I$ |

TABLE VII. Equation of state for the 5 LTHS model from $NpT$ MC simulations (compression route). The reduced pressure $p^*$ is defined as $p^* = p\sigma^3/(kT)$, $Z$ stands for the compressibility factor, $y$ for the volume fraction, $S_2$ for the order parameter. The phases have been labeled as Sm A (smectic A).

| $p^*$ | $y$ | $Z$ | $S_2$ | No. molecules | Phase |
|---|---|---|---|---|---|
| 2.4 | 0.420 | 14.94 | 0.90 | 144 | Sm A |
| 2.6 | 0.434 | 15.67 | 0.93 | 144 | Sm A |
| 2.8 | 0.447 | 16.39 | 0.94 | 144 | Sm A |
| 3.0 | 0.457 | 17.19 | 0.95 | 144 | Sm A |
| 3.2 | 0.471 | 17.78 | 0.96 | 144 | Sm A |
| 3.4 | 0.484 | 18.40 | 0.97 | 144 | Sm A |
| 3.6 | 0.496 | 19.02 | 0.97 | 144 | Sm A |
| 3.8 | 0.514 | 19.36 | 0.99 | 144 | Sm A |
| 4.0 | 0.528 | 19.84 | 0.99 | 144 | Sm A |

TABLE VIII. Equation of state for the 6 LTHS model from $NpT$ MC simulations (expansion route). The reduced pressure $p^*$ is defined as $p^* = p\sigma^3/(kT)$, $Z$ stands for the compressibility factor, $y$ for the volume fraction, $S_2$ for the order parameter. The different phases have been labeled as $I$ (isotropic), $N$ (nematic), and Sm A (smectic A), and $K$ (crystalline solid).

| $p^*$ | $y$ | $Z$ | $S_2$ | No. molecules | Phase |
|---|---|---|---|---|---|
| 130.0 | 0.734 | 556.75 | 0.99 | 144 | $K$ |
| 110.0 | 0.733 | 471.70 | 0.99 | 144 | $K$ |
| 90.0 | 0.731 | 386.93 | 0.99 | 144 | $K$ |
| 70.0 | 0.728 | 302.11 | 0.99 | 144 | $K$ |
| 50.0 | 0.723 | 217.20 | 0.99 | 144 | $K$ |
| 40.0 | 0.719 | 174.75 | 0.99 | 144 | $K$ |
| 30.0 | 0.713 | 132.22 | 0.99 | 144 | $K$ |
| 20.0 | 0.699 | 89.89 | 0.99 | 144 | $K$ |
| 15.0 | 0.687 | 68.59 | 0.99 | 144 | $K$ |
| 10.0 | 0.661 | 47.51 | 0.99 | 144 | $K$ |
| 9.00 | 0.655 | 43.17 | 0.99 | 144 | $K$ |
| 8.00 | 0.645 | 38.99 | 0.99 | 144 | $K$ |
| 7.00 | 0.632 | 34.79 | 0.99 | 144 | $K$ |
| 6.00 | 0.619 | 30.47 | 0.99 | 144 | $K$ |
| 5.00 | 0.600 | 26.16 | 0.99 | 144 | $K$ |
| 4.80 | 0.597 | 25.28 | 0.99 | 144 | $K$ |
| 4.60 | 0.588 | 24.56 | 0.99 | 144 | $K$ |
| 4.40 | 0.584 | 23.68 | 0.99 | 144 | $K$ |
| 4.20 | 0.575 | 22.95 | 0.99 | 144 | $K$ |
| 4.00 | 0.572 | 21.98 | 0.99 | 144 | $K$ |
| 3.80 | 0.565 | 21.11 | 0.99 | 144 | $K$ |
| 3.60 | 0.556 | 20.33 | 0.99 | 144 | $K$ |
| 3.40 | 0.550 | 19.42 | 0.99 | 144 | $K$ |
| 3.20 | 0.535 | 18.80 | 0.99 | 144 | $K$ |
| 3.00 | 0.526 | 17.91 | 0.99 | 144 | $K$ |
| 2.80 | 0.504 | 17.45 | 0.99 | 144 | $K$ |
| 2.60 | 0.491 | 16.63 | 0.99 | 144 | $K$ |
| 2.40 | 0.455 | 16.57 | 0.93 | 144 | Sm A |
| 2.20 | 0.440 | 15.73 | 0.94 | 144 | Sm A |
| 2.00 | 0.424 | 14.80 | 0.89 | 144 | Sm A |
| 1.80 | 0.407 | 13.91 | 0.92 | 144 | Sm A |
| 1.65 | 0.381 | 13.59 | 0.89 | 144 | Sm A |
| 1.60 | 0.357 | 14.07 | 0.75 | 144 | $N$ |
| 1.55 | 0.346 | 14.07 | 0.40 | 144 | $N$ |
| 1.50 | 0.338 | 13.95 | 0.35 | 144 | $N/I$ |
| 1.40 | 0.334 | 13.18 | 0.34 | 144 | $N/I$ |
| 1.35 | 0.327 | 12.96 | 0.20 | 144 | $I$ |
| 1.30 | 0.321 | 12.72 | 0.24 | 144 | $I$ |
| 1.25 | 0.308 | 12.75 | 0.16 | 144 | $I$ |
| 1.20 | 0.302 | 12.49 | 0.24 | 144 | $I$ |
| 1.20 | 0.310 | 12.15 | 0.22 | 144 | $I$ |
| 1.00 | 0.288 | 10.89 | 0.12 | 144 | $I$ |
| 0.80 | 0.263 | 9.57 | 0.11 | 144 | $I$ |
| 0.60 | 0.237 | 7.96 | 0.10 | 144 | $I$ |

TABLE IX. Equation of state for the 6 LTHS model from $NpT$ MC simulations (compression route). The reduced pressure $p^*$ is defined as $p^* = p\sigma^3/(kT)$, $Z$ stands for the compressibility factor, $y$ for the volume fraction, $S_2$ for the order parameter. The different phases have been labeled as $I$ (isotropic), $N$ (nematic), Sm A (smectic A), and $K$ (crystalline solid). The horizontal line divides the results for the $N=144$ results from the $N=320$ results.

| $p^*$ | $y$ | $Z$ | $S_2$ | No. molecules | Phase |
|---|---|---|---|---|---|
| 0.1 | 0.109 | 2.88 | 0.09 | 144 | $I$ |
| 0.2 | 0.152 | 4.13 | 0.11 | 144 | $I$ |
| 0.4 | 0.205 | 6.14 | 0.08 | 144 | $I$ |
| 0.6 | 0.244 | 7.74 | 0.09 | 144 | $I$ |
| 0.8 | 0.265 | 9.50 | 0.10 | 144 | $I$ |
| 0.9 | 0.276 | 10.26 | 0.10 | 144 | $I$ |
| 1.0 | 0.287 | 10.94 | 0.08 | 144 | $I$ |
| 1.1 | 0.296 | 11.68 | 0.09 | 144 | $I$ |
| 1.2 | 0.306 | 12.31 | 0.11 | 144 | $I$ |
| 1.3 | 0.315 | 12.96 | 0.19 | 144 | $I$ |
| 1.4 | 0.325 | 13.53 | 0.22 | 144 | $I$ |
| 1.6 | 0.348 | 14.43 | 0.48 | 144 | $N$ |
| 1.8 | 0.376 | 15.05 | 0.54 | 144 | $N$ |
| 0.30 | 0.182 | 5.18 | 0.08 | 320 | $I$ |
| 0.80 | 0.264 | 9.51 | 0.09 | 320 | $I$ |
| 1.00 | 0.287 | 10.96 | 0.06 | 320 | $I$ |
| 1.20 | 0.305 | 12.36 | 0.09 | 320 | $I$ |
| 1.30 | 0.317 | 12.89 | 0.10 | 320 | $I$ |
| 1.40 | 0.325 | 13.52 | 0.31 | 320 | $I/N$ |
| 1.45 | 0.332 | 13.71 | 0.19 | 320 | $N$ |
| 1.50 | 0.338 | 13.94 | 0.30 | 320 | $N$ |
| 1.55 | 0.340 | 14.34 | 0.19 | 320 | $N$ |
| 1.60 | 0.343 | 14.67 | 0.35 | 320 | $N$ |
| 1.65 | 0.349 | 14.84 | 0.54 | 320 | $N$ |
| 1.70 | 0.356 | 15.01 | 0.63 | 320 | $N$ |
| 1.75 | 0.368 | 14.94 | 0.76 | 320 | $N$ |
| 1.80 | 0.374 | 15.14 | 0.79 | 320 | $N$ |
| 1.85 | 0.392 | 14.83 | 0.93 | 320 | $N$/Sm A |
| 1.95 | 0.409 | 15.00 | 0.93 | 320 | Sm A |
| 2.05 | 0.418 | 15.42 | 0.93 | 320 | Sm A |
| 2.10 | 0.422 | 15.65 | 0.93 | 320 | Sm A |
| 2.20 | 0.429 | 16.10 | 0.94 | 320 | Sm A |
| 2.30 | 0.440 | 16.44 | 0.92 | 320 | Sm A |
| 2.40 | 0.444 | 16.99 | 0.93 | 320 | Sm A |
| 2.50 | 0.449 | 17.48 | 0.93 | 320 | Sm A |
| 2.60 | 0.459 | 17.81 | 0.92 | 320 | Sm A |
| 2.65 | 0.459 | 18.12 | 0.93 | 320 | Sm A |
| 2.70 | 0.466 | 18.22 | 0.94 | 320 | Sm A |
| 2.75 | 0.463 | 18.66 | 0.94 | 320 | Sm A |
| 2.80 | 0.471 | 18.67 | 0.95 | 320 | Sm A |
| 2.85 | 0.474 | 18.88 | 0.96 | 320 | Sm A |
| 2.90 | 0.481 | 18.94 | 0.96 | 320 | Sm A |
| 2.95 | 0.492 | 18.83 | 0.97 | 320 | Sm A |
| 3.00 | 0.497 | 18.96 | 0.97 | 320 | Sm A |

phase transition we took a state point ($p^*=2.4$, $y=0.420$) from the expansion branch and then subjected it to a series of compression simulations (see Table VII). If the solid–smectic A were second order we should expect to see a return to the solid branch. However we see no such return and thus conclude that the solid–smectic A phase transition is first order.

### D. The $m=6$ case

For the hexamer model we observe the following phase behavior; on expansion (see Table VIII) the solid phase is

TABLE X. Equation of state for the 6 LTHS model from $NpT$ MC simulations (compression route). The reduced pressure $p^*$ is defined as $p^* = p\sigma^3/(kT)$, $Z$ stands for the compressibility factor, $y$ for the volume fraction, $S_2$ for the order parameter. The phases have been labeled as Sm A (smectic A).

| $p^*$ | $y$ | $Z$ | $S_2$ | No. molecules | Phase |
|---|---|---|---|---|---|
| 2.4 | 0.457 | 16.48 | 0.91 | 144 | Sm A |
| 2.6 | 0.467 | 17.51 | 0.92 | 144 | Sm A |
| 2.8 | 0.480 | 18.32 | 0.92 | 144 | Sm A |
| 3.0 | 0.491 | 19.21 | 0.96 | 144 | Sm A |
| 3.2 | 0.506 | 19.86 | 0.97 | 144 | Sm A |
| 3.4 | 0.515 | 20.76 | 0.97 | 144 | Sm A |
| 3.6 | 0.523 | 21.63 | 0.96 | 144 | Sm A |
| 3.8 | 0.538 | 22.21 | 0.98 | 144 | Sm A |
| 4.0 | 0.552 | 22.78 | 0.94 | 144 | Sm A |

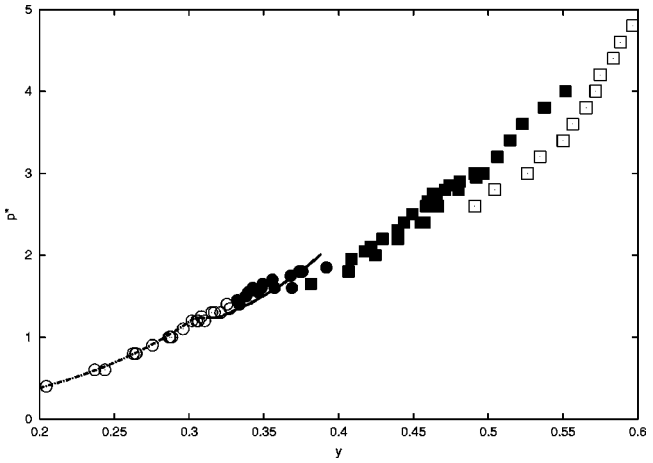


FIG. 5. Plot of the EOS for the 6 LTHS model. ⊙ represents isotropic state points, ● represents nematic state points, ■ represents smectic state points, and ⊡ represents solid state points. The dotted–dashed curve is the Vega–Lago theory for the isotropic phase, the dashed line represents the tie line, and the solid curve for the nematic phase.

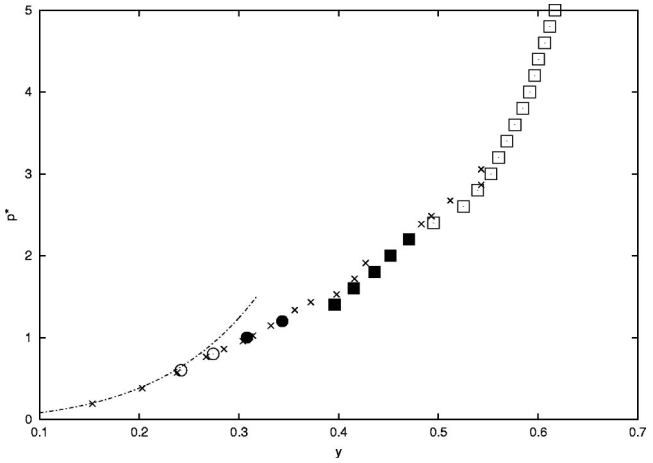


FIG. 6. Plot of the EOS for the 7 LTHS model. ⊙ represents isotropic state points, ● represents nematic state points, ■ represents smectic state points, and ⊡ represents solid state points. × are the results from Williamson and Jackson. The dotted–dashed curve is the TPT1 EOS.

TABLE XI. Equation of state for the 7 LTHS model from $NpT$ MC simulations (expansion route). The reduced pressure $p^*$ is defined as $p^* = p\sigma^3/(kT)$, $Z$ stands for the compressibility factor, $y$ for the volume fraction, $S_2$ for the order parameter. The different phases have been labeled as $I$ (isotropic), $N$ (nematic), Sm A (smectic A), and $K$ (crystalline solid).

| $p^*$ | $y$ | $Z$ | $S_2$ | No. molecules | Phase |
|---|---|---|---|---|---|
| 6.0 | 0.634 | 34.66 | 0.99 | 144 | $K$ |
| 5.0 | 0.617 | 29.71 | 0.99 | 144 | $K$ |
| 4.8 | 0.612 | 28.76 | 0.99 | 144 | $K$ |
| 4.6 | 0.607 | 27.79 | 0.99 | 144 | $K$ |
| 4.4 | 0.600 | 26.86 | 0.99 | 144 | $K$ |
| 4.2 | 0.597 | 25.80 | 0.99 | 144 | $K$ |
| 4.0 | 0.592 | 24.78 | 0.99 | 144 | $K$ |
| 3.8 | 0.585 | 23.82 | 0.99 | 144 | $K$ |
| 3.6 | 0.577 | 22.87 | 0.99 | 144 | $K$ |
| 3.4 | 0.569 | 21.91 | 0.99 | 144 | $K$ |
| 3.2 | 0.560 | 20.93 | 0.99 | 144 | $K$ |
| 3.0 | 0.553 | 19.89 | 0.99 | 144 | $K$ |
| 2.8 | 0.540 | 19.02 | 0.99 | 144 | $K$ |
| 2.6 | 0.525 | 18.14 | 0.99 | 144 | $K$ |
| 2.4 | 0.495 | 17.76 | 0.99 | 144 | $K$ |
| 2.2 | 0.471 | 17.13 | 0.97 | 144 | Sm A |
| 2.0 | 0.452 | 16.22 | 0.94 | 144 | Sm A |
| 1.8 | 0.436 | 15.14 | 0.94 | 144 | Sm A |
| 1.6 | 0.415 | 14.12 | 0.92 | 144 | Sm A |
| 1.4 | 0.396 | 12.96 | 0.93 | 144 | Sm A |
| 1.2 | 0.343 | 12.81 | 0.87 | 144 | $N$ |
| 1.0 | 0.308 | 11.90 | 0.64 | 144 | $N$ |
| 0.8 | 0.274 | 10.70 | 0.23 | 144 | $I$ |
| 0.6 | 0.242 | 9.09 | 0.11 | 144 | $I$ |

stable down to $y=0.491$, we have a smectic A phase in the range $(0.381 \leqslant y \leqslant 0.455)$, and a nematic phase in the range $(0.334 \leqslant y \leqslant 0.357)$. At $y=0.327$ the system becomes isotropic. Upon compression (Table IX) of the isotropic fluid we find an isotropic–nematic transition at $y=0.332$, followed by a nematic–smectic A transition at $y=0.392$. In a similar manner to the $m=5$ model, a short series of compression runs were performed starting from the smectic phase at $p^*=2.4$, $y=0.457$ (see Table X) obtained from the expansion run. These compression runs show a region of hysteresis, strongly indicating that the Smectic A–solid transition is first order. It is more difficult to assess the order of the nematic–Smectic A phase transition, but narrow range of hysteresis can be observed in Fig. 5 suggesting that this is also a first order phase transition.

In Fig. 5, as well as the state points, we plot the lines for the Vega–Lago theory for the isotropic–nematic transition. It can be seen that the theory slightly underestimates the densities and pressures for the location of the transition.

### E. The $m=7$ case

For the $m=7$ model we have studied the expansion of the solid phase for $N=144$ particles. The $m=7$ model has already been considered in detail in an extensive study by Williamson and Jackson.[14] These state points were simulated in order to gauge the influence of system size on the results; in the work of Williamson and Jackson $N=576$ molecules.

It can be seen from Fig. 6 and Table XI that our results for the EOS and phase behavior are in close agreement with those of Williamson and Jackson, and that finite size effects are minimal. In summary the initial solid phase was found to be stable down to $y=0.495$, which then melted into the liquid crystal smectic A phase $(0.396 \leqslant y \leqslant 0.495)$, followed by a nematic region $(0.308 \leqslant y \leqslant 0.343)$. Below $y=0.274$ we find the isotropic fluid. The theoretical prediction for the location of the isotropic–nematic transition, at $p^*=0.82$, corresponds rather well with the location of the transition found on expansion, at $0.8 \leqslant p^* \leqslant 1.0$.

## IV. CONCLUSION

In our view the main conclusions that can be drawn from this work can be summarized as follows.

No liquid crystal phases are found for the models $m=3$ and $m=4$.

The first occurrence of liquid crystal formation, a smectic A phase, is found for the $m=5$ model. This brings the aspect ratio to a lower limit of 5, rather than the value of 6 monomer units proposed by Flory.

The $m=6$ and $m=7$ models demonstrate both nematic and smectic A phases.

Phase transitions for the LTHS model appear to be first order.

Wertheim's TPT1 provides a good description of the low density isotropic fluid; however, it overestimates the pressure at higher packing fractions.

The Vega–Lago theory used along with TPT1 EOS for the isotropic phase yields fair estimates of the isotropic–nematic transition for the LTHS model.

## ACKNOWLEDGMENTS

Financial support is due to project No. BFM2001-1420-C02-01 of the Spanish MCyT (Dirección General de Investigación, Ministerio de Ciencia y Tecnología). One of the authors (C.M.), would like to acknowledge and thank the European Union FP5 Program for the award of a Marie Curie post-doctoral fellowship (No. HPMF-CT-1999-00163). We wish to thank the "Centro de Supercomputacion" of Universidad Complutense de Madrid for a generous allocation of computer time on their SGI Origin 2000. We also thank Julio Largo for generating the close packing structures of the LTHS models considered in this work.

[1] L. Onsager, Ann. N.Y. Acad. Sci. **51**, 627 (1949).
[2] P. J. Flory, Proc. R. Soc. London, Ser. A **234**, 73 (1956).
[3] A. Chamoux and A. Perera, Mol. Phys. **93**, 649 (1998).
[4] D. Frenkel, J. Phys. Chem. **92**, 3280 (1988).
[5] G. T. Evans, Mol. Phys. **87**, 239 (1996).
[6] S. C. McGrother, D. C. Williamson, and G. Jackson, J. Chem. Phys. **104**, 6755 (1996).
[7] P. Bolhuis and D. Frenkel, J. Chem. Phys. **106**, 666 (1997).
[8] D. Frenkel and B. M. Mulder, Mol. Phys. **55**, 1171 (1985).
[9] P. J. Camp and M. P. Allen, J. Chem. Phys. **106**, 6681 (1997).
[10] M. Whittle and A. J. Masters, Mol. Phys. **72**, 247 (1991).
[11] K. M. Jaffer, S. B. Opps, and D. E. Sullivan, J. Chem. Phys. **110**, 11630 (1999).
[12] A. Yethiraj and H. Fynewever, Mol. Phys. **93**, 693 (1998).
[13] H. Fynewever and A. Yethiraj, J. Chem. Phys. **108**, 1636 (1998).
[14] D. C. Williamson and G. Jackson, J. Chem. Phys. **108**, 10294 (1998).
[15] M. R. Wilson, Mol. Phys. **85**, 193 (1995).
[16] M. R. Wilson and M. P. Allen, Mol. Phys. **80**, 277 (1993).
[17] M. R. Wilson, Mol. Phys. **81**, 675 (1994).
[18] M. S. Wertheim, J. Chem. Phys. **87**, 7323 (1987).

[19] W. G. Chapman, G. Jackson, and K. E. Gubbins, Mol. Phys. **65**, 1 (1988).
[20] C. Vega and S. Lago, J. Chem. Phys. **100**, 6727 (1994).
[21] C. Vega, S. Lago, and B. Garzon, Mol. Phys. **82**, 1233 (1994).
[22] D. C. Williamson and G. Jackson, Mol. Phys. **86**, 819 (1995).
[23] M. P. Allen and D. J. Tildesley, *Computer Simulation of Liquids* (Oxford University Press, Oxford, 1987).
[24] C. Vega, E. P. A. Paras, and P. A. Monson, J. Chem. Phys. **96**, 9060 (1992).
[25] P. Najafabadi and S. Yip, Scr. Metall. **17**, 1199 (1983).
[26] S. Yashonath and C. N. R. Rao, Mol. Phys. **54**, 245 (1985).
[27] R. Eppenga and D. Frenkel, Mol. Phys. **52**, 1303 (1984).
[28] M. R. Wilson, J. Mol. Liq. **68**, 23 (1996).
[29] M. D. Amos and G. Jackson, Mol. Phys. **74**, 191 (1991).
[30] E. A. Müller and K. E. Gubbins, Mol. Phys. **80**, 957 (1993).
[31] T. Boublik, C. Vega, and M. Diaz-Peña, J. Chem. Phys. **93**, 730 (1990).